

**Light-triggered Explosion of Lipid Vesicles**

Journal:	<i>Soft Matter</i>
Manuscript ID	SM-ART-06-2020-001027.R1
Article Type:	Paper
Date Submitted by the Author:	25-Jul-2020
Complete List of Authors:	Malik, Vinit; University of Illinois at Urbana-Champaign, Mechanical Science and Engineering Shin, Sangwoo; University of Hawai'i at Manoa, Department of Mechanical Engineering Feng, Jie; University of Illinois at Urbana-Champaign, Mechanical Science and Engineering

Cite this: DOI: 00.0000/xxxxxxxxxx

## Light-triggered Explosion of Lipid Vesicles<sup>†</sup>

Vinit Kumar Malik,<sup>a</sup> Sangwoo Shin,<sup>b</sup> and Jie Feng<sup>\*a</sup>

Received Date

Accepted Date

DOI: 00.0000/xxxxxxxxxx

Lipid vesicles have received considerable interest because of their applications to *in vitro* reductionist cell membrane models as well as therapeutic delivery vehicles. In these contexts, the mechanical response of vesicles in nonequilibrium environments plays a key role in determining the corresponding dynamics. A common understanding of the response of lipid vesicles upon exposure to a hypotonic solution is a characteristic pulsatile behavior. Recent experiments, however, have shown vesicles exploding under an osmotic shock generated by photo-reactions, yet the explanatory mechanism is unknown. Here we present a generalized biophysical model incorporating a stochastic account of membrane rupture to describe both swell-burst-reseal cycling and exploding dynamics. This model agrees well with experimental observations, and it unravels that the sudden osmotic shock strains the vesicle at an extreme rate, driving the vesicle into buckling instabilities responsible for membrane fragmentation, *i.e.* explosion. Our work not only advances the fundamental framework for non-equilibrium vesicle dynamics under osmotic stress, but also offers design guidelines for programmable vesicle-encapsulated substance release in therapeutic carriers.

### 1 Introduction

Giant unilamellar vesicles (GUVs) are commonly employed as a simple representative system to study biological cell behaviors. In addition, with the development of biological techniques and use of bottom-up approaches, GUVs also serve as fundamental building blocks to construct a cell-mimicking system<sup>1</sup>. Therefore, GUVs are considered as an excellent tool for enhancing a fundamental understanding of lipid membranes and artificial cells ranging from studying phase separation and lipid domain emergence<sup>2</sup> to modeling physiological response of cells to their extracellular environment<sup>3,4</sup>. In these contexts, the mechanical response of vesicles plays a key role in predicting shape transformation of cells<sup>5</sup>, illuminating the origins of life<sup>6</sup>, and determining the content release dynamics in targeted nanotherapeutics<sup>7</sup>; leaving vesicle stability in nonequilibrium environments an indispensable aspect of the dynamics. In particular, osmoregulatory has a significant effect on vesicle stability, sometimes leading to drastic outcomes such as fusion and fission of cells and liposomes<sup>8,9</sup>. Hence, vesicles response under osmotic stress has been a topic of interest in the soft matter community for decades<sup>10–15</sup>. For instance, as illustrated in Fig. 1a, a vesicle swollen due to hypotonicity

will relax following initial bursting, subsequently resealing owing to the excess pore edge energy. This cycle of swell-burst-reseal continues until the osmotic gradient drops below a value that the vesicle membrane can withstand.

Recently, light-induced osmotic shock has been used to trigger catastrophic lysis of micro-scale vesicles, resulting in rapid release of inner contents<sup>16,17</sup> in contrast to continuous pulsatile behavior<sup>18</sup>. During rupture under such conditions, formation of only a single pore in the vesicle membrane has been observed<sup>17</sup>. We refer this scenario as “exploding”, in which the vesicle becomes unstable, with the membrane fragmenting into daughter structures as shown in Fig. 1b. It has been suggested that photo-chemical reactions of encapsulated photoactive materials lead to a sudden increase of osmotic imbalance, as an “active osmotic gradient”, causing vesicle explosion<sup>16</sup>. Nonetheless, a general framework that allows the bifurcation of vesicle dynamics into either swell-burst-reseal cycling (Fig. 1a) or exploding (Fig. 1b) has not been explicated so far (see Table S1 for a summary of previous literatures). Such questions arise not only in vesicle osmoregulation, but also in other important scenarios, such as osmosensing and osmosignaling in living cells. In addition, the selective and rapid release of entrapped species from various compartments in artificial cells is another example where such a framework can provide guidelines in a soft matter system<sup>19</sup>.

Here we develop a general biophysical model for the osmotic response of vesicles under the light-triggered osmotic shock, integrating stochastic poration of the membrane, continuum transport and light-induced reactions. We first present a stochastic account of membrane poration in order to accommodate strain-rate-

<sup>a</sup> Department of Mechanical Science and Engineering, University of Illinois at Urbana-Champaign, Urbana, Illinois 61801, USA E-mail: jiefeng@illinois.edu

<sup>b</sup> Department of Mechanical Engineering, University of Hawaii at Manoa, Honolulu, Hawaii 96822, USA

<sup>†</sup> Electronic Supplementary Information (ESI) available: [details of any supplementary information available should be included here]. See DOI: 10.1039/cXsm00000x/

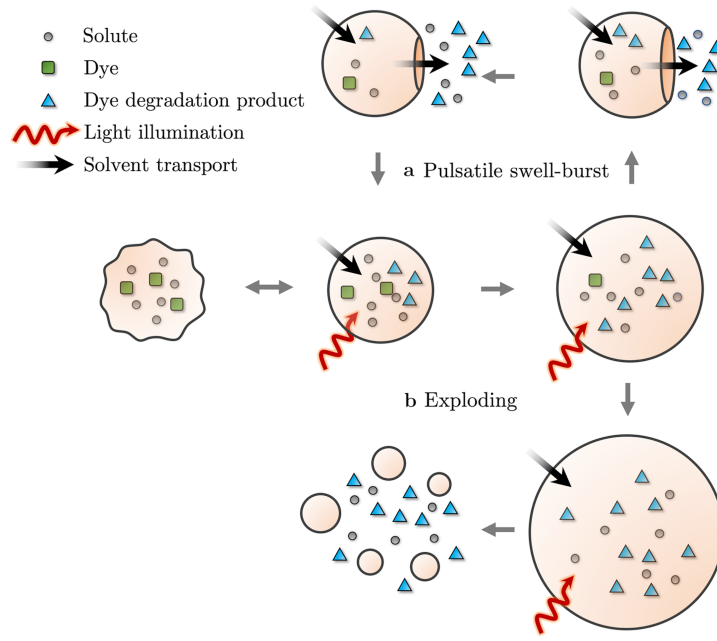


**Fig. 1 Schematic for the dynamic response of a lipid vesicle under an active osmotic gradient.** A vesicle may follow two experimentally observed paths under an active osmotic gradient: (a) Pulsatile swell-burst-reseal cycling, in which the pore forms and reseals cyclically until the membrane can withstand the residual osmotic pressure; (b) Exploding, in which the vesicle explodes along with the formation of smaller daughter structures.

dependent responses of the lipid membrane. Next, we develop a vesicle model based on Helfrich's curvature elasticity using a Lagrangian framework to account for viscous dissipation, which captures the essential quantitative features for pulsatile vesicle dynamics. Then we account for light-triggered chemical reaction and discuss vesicles explosion with our model. The model's prediction is in good agreement with experimental observations of vesicle explosion. Finally, we discuss the bifurcation conditions under which irreversible exploding is favorable.

## 2 Model

### 2.1 Stochastic approach for pore formation

Even in a relaxed state, lipid membranes spontaneously form prepores (*i.e.* metastable hydrophilic defects) as a result of non-uniform membrane lipid density due to thermal fluctuations. For a prepore to become unstable and transition into a pore, it must overcome two energy barriers: the nucleation energy barrier  $\Delta E_n$ , and the cavitation energy barrier  $\Delta E_c$ <sup>20,21</sup>. At low membrane tension,  $\Delta E_c$  dominates  $\Delta E_n$ , and thus controls the distribution of the membrane lytic tension,  $\sigma_l$ , under external stress. However, above the cross-over membrane tension,  $\Delta E_n$  determines the membrane failure rate. Only recently, a stochastic approach has been considered for incorporating a strain-rate-dependant response to osmotic stress, using the Langevin approach to model pore formation<sup>15</sup>. However, that model has not included  $\Delta E_n$ , and hence is only suitable for small tension loading rates and low membrane tension. Photo-assisted chemical reactions, in contrast, can induce a large osmotic gradient rapidly, causing a very high loading rate,  $\dot{\sigma}$ .

To account for the strain-dependent response in both scenar-

ios, we propose a generalized model for pore formation. We determine  $\sigma_l$  by introducing a semi-analytic technique of combining the kinetics of membrane rupture with vesicle dynamics through a Monte-Carlo sampling approach. Following Evans and Smith<sup>22</sup>, the survival probability of the vesicle membrane  $S(\sigma)$  under a constant  $\dot{\sigma}$  is formulated as

$$\frac{dS(\sigma)}{d\sigma} = \frac{-k_{hole}}{\dot{\sigma}} S(\sigma). \quad (1)$$

Here,  $k_{hole}$  is the frequency of prepore occurrences which depends on  $\dot{\sigma}$ , line tension  $\gamma$ , and the lateral membrane tension  $\sigma$ . The dependence of membrane rupture probability on  $\Delta E_n$  and  $\Delta E_c$  is inherently embedded in the expression of  $k_{hole}$ <sup>22</sup>. To get a direct relationship between survival probability  $S(\sigma)$  and  $\sigma$ , Eq. 1 is written in terms of  $\sigma$  through a variable change  $\sigma = \dot{\sigma}t$  and solved with the initial condition,  $S(0) = 1$ . Figures 2a and b illustrate a typical stochastic process of pore formation presenting the probability density of rupture  $p_r = -dS(\sigma)/d\sigma$  (solid red curve, Fig. 2a), and the probability distributions of  $\sigma_l$  under different loading rates (Fig. 2b). Importantly, these plots illustrate that the most probable  $\sigma_l$  increases with  $\dot{\sigma}$ . To determine  $\sigma_l$  for each swell-burst cycle, samples are drawn from the probability distribution informed by  $\dot{\sigma}$  using a Monte-Carlo approach (100 draws, for details see SI section II). We overlay a kernel density estimation (KDE) of sampled  $\sigma_l$  with  $p_r$  to show the underlying probability distribution (Fig. 2a). The good agreement between true distribution and KDE confirms the feasibility of such an algorithm to determine the membrane rupture events of vesicles under osmotic stress. The probability distribution with respect to various loading rates will be used to determine the most probable  $\sigma_l$  for later discussion as well as the comparison with the experiments.

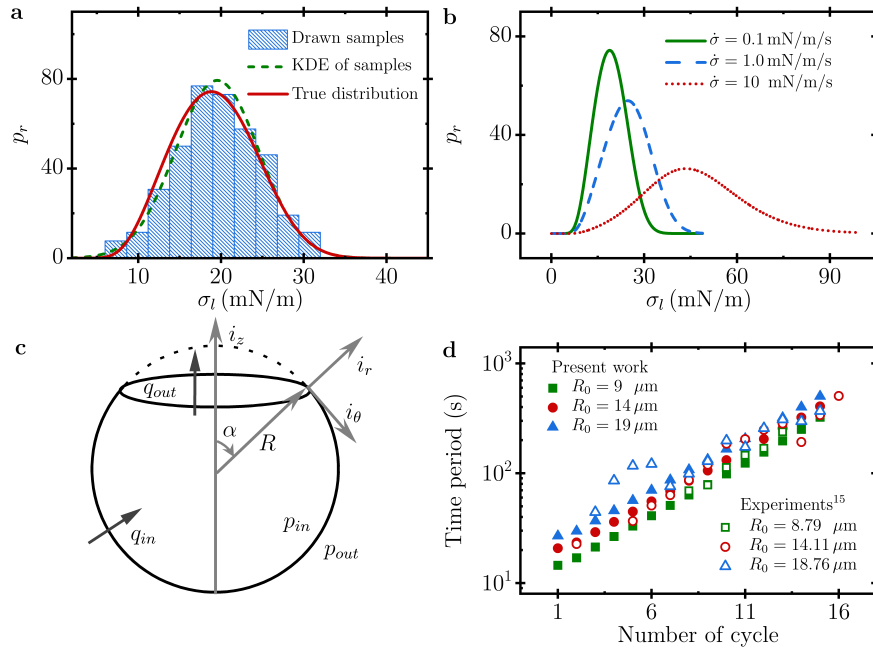


**Fig. 2 Stochastic kinetics of hole nucleation in a lipid membrane.** (a) Probability density of membrane rupture. The red solid line represents a true probability distribution obtained from the numerical solution of Eq. 1 (for  $\dot{\sigma} = 0.1$  mN/m/s). The blue histogram shows samples drawn from the true distribution (100 draws). The green dashed line shows a Gaussian kernel density estimation (KDE) of the drawn samples. (b) Probability density of membrane rupture under different  $\dot{\sigma}$ . The distribution of membrane lytic tension shifts towards the right with increasing  $\dot{\sigma}$ . (c) Geometrical schematic of the vesicle model.  $R$  is the instantaneous radius of a vesicle, and  $\alpha$  is the angle subtended by the pore at the center.  $\Delta p = p_{in} - p_{out}$  is the Laplace pressure jump. The arrows show the mass transport in ( $q_{in}$ ) and out ( $q_{out}$ ) of the vesicle. (d) Model comparison with the pulsatile experiments<sup>15</sup>. (see Table S2 for the material properties used in the simulation)

## 2.2 Pore evolution

To model vesicle dynamics, we employ the Helfrich's spontaneous curvature-elasticity framework which allows us to include the effect of spontaneous curvature,  $H_s$ <sup>23</sup>. The spontaneous (or intrinsic) curvature  $H_s$  is defined as the preferred curvature of the lipid bilayer for which the bending energy is minimum<sup>24</sup>. For a symmetric lipid bilayer system,  $H_s = 0$ , although it can be non-zero if the lipid bilayers are facing different solute species or concentrations<sup>25,26</sup>. The total energy,  $E$ , of the vesicle system can be written as

$$E = 2\pi\gamma R \sin\alpha + \frac{\sigma^2}{2K} A_0 + \frac{1}{2} k_b \int_A (H - H_s)^2 dA - \int_{R_0}^R \Delta p 2\pi R^2 (1 + \cos\alpha) dR. \quad (2)$$

In writing Eq. 2, we assume a spherical geometry of the vesicle with a single circular pore embedded in it (Fig. 2c). Here we use the instantaneous radius,  $R$ , and the angle subtended by the pore at the center,  $\alpha$ , as our configuration space, while  $R_0$ ,  $A_0$ ,  $A$ ,  $K$ , and  $k_b$  are the vesicle's initial radius, initial area, instantaneous area, membrane compressibility coefficient, and bending rigidity respectively. The total energy  $E$  in Eq. 2, is comprised of energy contributions from the pore edge<sup>10</sup>, membrane stretching<sup>25</sup> and bending<sup>23</sup> as well as the work done by pressure due to changes in the volume of the system. Differing forms of Eq. 2 have been used in the theoretical frameworks ranging from interpreting shape fluctuations in the spectra of microemulsions and

vesicles<sup>27</sup> to understanding phase separation dynamics of vesicles<sup>28–30</sup>.

As the membrane relaxes upon rupture, the energy is dissipated by viscous forces in both the membrane<sup>12,13,31</sup> and the surrounding fluid<sup>32,33</sup>. During the pore lifetime, we account for viscous damping through a Rayleigh dissipation function as

$$\Phi = \pi C_1 \eta_s R \sin\alpha R^2 \dot{\alpha}^2 + 2\pi C_2 \eta_m d R^2 \dot{\alpha}^2, \quad (3)$$

where  $C_1$  and  $C_2$  are geometric coefficients coming from a detailed flowfield solution in a recent study<sup>34</sup>.  $\eta_s$ ,  $\eta_m$ , and  $d$  are the solvent viscosity, membrane viscosity, and membrane thickness respectively. The first term on the right hand side of Eq. 3, represents the viscous losses due to a relaxing membrane imparting motion to the surrounding fluid while the second term accounts for the internal membrane viscous losses. In Eq. 3, the viscous dissipation due to dilation, *i.e.*  $\dot{R}$ , is neglected. We treat Eqs. 2 and 3 in the Lagrangian framework with non-conservative forces, while neglecting inertia, to obtain the governing equations for evolution of vesicle system as

$$\frac{1}{R} \frac{\partial E}{\partial \alpha} = - \frac{\partial \Phi}{\partial (R\dot{\alpha})}, \quad (4a)$$

$$\frac{\partial E}{\partial R} = - \frac{\partial \Phi}{\partial \dot{R}}. \quad (4b)$$

Equation 4a gives the governing equation for pore evolution as

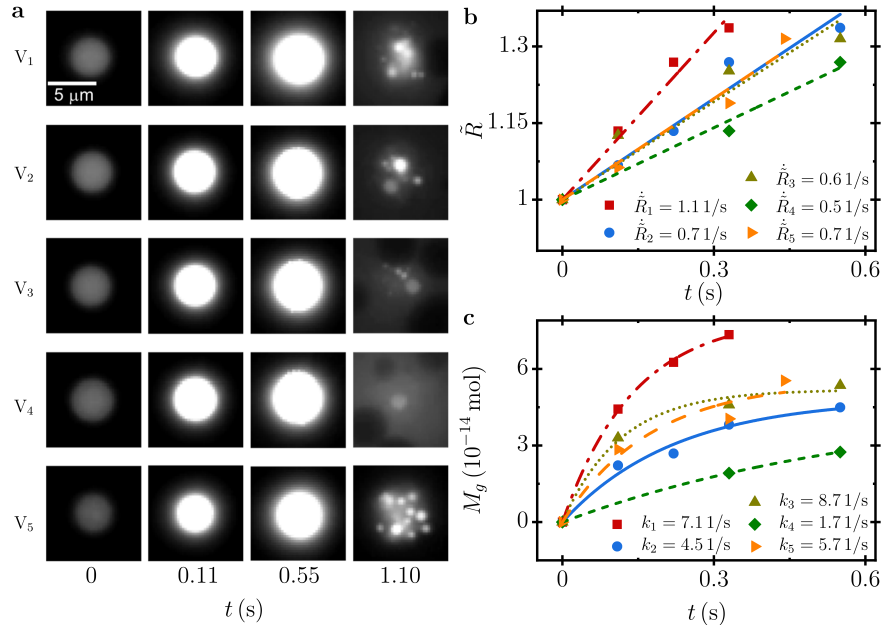


**Fig. 3 Experimental data extraction for the light-triggered exploding of vesicles.** (a) Experimental images from Zhu and Szostak<sup>16</sup>.  $V_i$  is the  $i^{\text{th}}$  vesicle. (b)  $\tilde{R} = R/R_0$  of the representative vesicles with respect to time. The lines passing through the symbols are a linear fit. (c) Total number of moles generated inside the vesicles as a function of time. The lines passing through the symbols represent an exponential fit of the form  $A(1 - e^{-k_i t})$ , where  $k_i$  is the chemical reaction rate constant obtained for the  $i^{\text{th}}$  vesicle.

simplified below

$$\left( C_1 R \sin \alpha + 2C_2 \eta_m d \right) \dot{\alpha} = \left( -\frac{\gamma \cos \alpha}{R} - \frac{2\sigma R_0^2}{KR^2} \frac{\partial \sigma}{\partial \alpha} + \frac{1}{2} k_b (H - H_s)^2 \sin \alpha \right). \quad (5)$$

Additionally, from Eq. 4b, we obtain a relation governing the excess pressure,  $\Delta p = p_{in} - p_{out}$ , as

$$\Delta p = \frac{\gamma \sin \alpha}{R^2 (1 + \cos \alpha)} + \frac{2\sigma R_0^2}{KR^2 (1 + \cos \alpha)} \frac{\partial \sigma}{\partial R} + k_b \left( \frac{H_s^2}{R} - \frac{2H_s}{R^2} \right), \quad (6)$$

using  $H = 2/R$  for a sphere. To compute  $\partial \sigma / \partial R$  and  $\partial \sigma / \partial \alpha$ , as presented in Rawicz et al.<sup>35</sup>, we use the constitutive relation between area strain  $\epsilon_a = A/A_0 - 1$  and membrane stress  $\sigma$  written as

$$\frac{2\pi R^2 (1 + \cos \alpha) - 4\pi R_0^2}{4\pi R_0^2} = \frac{k_B T}{8\pi k_b} \ln \left( 1 + \frac{\sigma A_s}{24\pi k_b} \right) + \frac{\sigma}{K}. \quad (7)$$

The term on the left hand side of Eq. 7 represents the area strain  $\epsilon_a$ , where we use the relation  $A = 2\pi R^2 (1 + \cos \alpha)$  for instantaneous surface area of the vesicle and  $A_0 = 4\pi R_0^2$  for the initial vesicle surface area. The first term on the right-hand side of Eq. 7 represents flattening of soft thermal undulations, while the second term takes account of the direct Hookean-like membrane stretching. During initial stretching, the undulation term dominates the membrane response, however the direct stretch term will dominate once the undulations are flattened out.

To incorporate stochasticity of pore nucleation in a membrane, we rewrite Eq. 5 to govern the nucleation and evolution of pore as below

$$\left( C_1 R \sin \alpha + 2C_2 \eta_m d \right) \dot{\alpha} = \left( -\frac{\gamma \cos \alpha}{R} - \frac{2\sigma R_0^2}{KR^2} \frac{\partial \sigma}{\partial \alpha} + \frac{1}{2} k_b (H - H_s)^2 \sin \alpha \right) \theta(\sigma - \sigma_l). \quad (8)$$

We use the Heaviside step function,  $\theta(\sigma - \sigma_l)$ , such that  $\dot{\alpha} = 0$  for  $\sigma < \sigma_l$ . Here, we obtain  $\sigma_l$  by sampling from the probability distribution (Fig. 2a) obtained by solving Eq. 1. Next, we will develop the governing equations for the vesicle radius  $R$  and osmotic difference across the membrane  $\Delta c$  respectively.

### 2.3 Mass conservation for solvent

As shown in Fig. 2c, the solvent flows into the vesicle ( $q_{in}$ ) as it experiences a hypotonic osmotic imbalance. At the same time, the inner contents of the vesicle leak out ( $q_{out}$ ) through the pore by the pressure jump,  $\Delta p$ . We utilize the continuity principle for the governing relation of  $R$  written as

$$\frac{dV}{dt} = q_{in} A - q_{out} A_p, \quad (9)$$

where  $V = \frac{\pi}{3} R^3 \left( 2 + \frac{9}{4} \cos \alpha - \frac{1}{4} \cos 3\alpha \right)$  represents the volume of the vesicle. Substituting the volume  $V$  in Eq. 9 and simplifying using trigonometry identities, we obtain

$$(A + A_p \cos \alpha) \dot{R} = q_{in} A - (q_{out} - R \dot{\alpha} \sin \alpha) A_p. \quad (10)$$

Here,  $A = 2\pi R^2(1 + \cos\alpha)$  denotes the surface area of the vesicle, and  $A_p = \pi R^2 \sin^2\alpha$  represents the area of the circular pore (Fig. 2c). Assuming low Reynolds number regime,  $\Delta p$  relates to the leak-out flow  $q_{out}$  as

$$q_{out} = \frac{\Delta p R \sin\alpha}{Q\eta_s}, \quad (11)$$

where  $Q$  is a geometric coefficient that generalizes the Sampson flow through a circular orifice embedded in a plane to a finite spherical geometry of the vesicle<sup>34</sup>. Using the Starling hypothesis<sup>36</sup>, we relate the solvent influx  $q_{in}$  as

$$q_{in} = P v_s \left( \Delta c - \frac{\Delta p}{R_G T} \right), \quad (12)$$

where  $P$  is the permeability coefficient of the lipid bilayer,  $\Delta c$  is the concentration difference across the membrane,  $v_s$  is the solvent molar volume, and  $R_G$  is the universal gas constant. From Eq. 11, the excess pressure  $\Delta p$  built up inside the vesicle drives the inner content out, thus helping the vesicle to fully relax. On the other hand, from Eq. 12,  $\Delta p$  opposes the solvent influx by countering the concentration difference  $\Delta c = c_{in} - c_{out}$  across the membrane.  $c_{in}$  and  $c_{out}$  are the inner and outer solute concentrations, respectively.

#### 2.4 Active osmotic gradient

In traditional osmotic stress experiments using GUVs,  $\Delta c$  is passively controlled by the continuum mass transport processes of the system. However, light-triggered reactions leverage chemical decomposition to generate an osmotic imbalance in presence of a photosensitizer. A photosensitizer absorbs photons, and thus becomes excited to singlet form. However, such a form is very short-lived, and it jumps to a triplet state which is stable enough to transfer energy to dissolved oxygen for production of a singlet oxygen<sup>37</sup>. The reactive oxygen species can further react in two ways: with a specific substrate, (e.g. Na-bicine<sup>16</sup>) or the photosensitizer itself<sup>17</sup>, which form new products inside the vesicle, and in turn induce an osmotic shock rapidly. Such photoreactions provide a ‘‘tunable’’ osmolar gradient in a spatio-temporally manner, which allows for either swell-burst cycling<sup>12,13</sup> or irreversible bursting<sup>16,17</sup>. Since osmolarity is a colligative property, it is necessary to account for the generation of solute molecules by light-triggered reactions.

When the deactivation constant of singlet oxygen via the solvent dominates the rate constants of chemical and physical quenching of singlet oxygen by the substrate, the rate of disappearance of a specific substrate obeys the first-order kinetics<sup>38</sup>. To account for solute molecule generation, we adopt a first-order kinetics for the photo-chemical reaction as

$$\left( \frac{dc_{sub}}{dt} \right)^* = -I\phi \frac{k_r}{k_d} c_{sub} \quad (13)$$

where  $c_{sub}$  is the substrate concentration,  $I$  is the intensity of the absorbed light,  $\phi$  is the quantum yield for singlet oxygen,  $k_r$  is the rate constant for chemical quenching by the substrate, and  $k_d$  is the deactivation coefficient by solvent molecules. Here we

neglect the mass transport in and out of the vesicle, and  $*$  denotes the concentration changes only due to the chemical reaction. The concentration of the product,  $j$ , follows

$$\left( \frac{dc_j}{dt} \right)^* = (Z_j^p) I\phi \frac{k_r}{k_d} c_{sub}. \quad (14)$$

Here,  $Z_j^p$  represents stoichiometric coefficients of  $j^{th}$  product while setting  $Z_{sub} = 1$ . Therefore, from Eqs. 13-14, the rate of total solute concentration due to the photo-chemical reaction is expressed as

$$\left( \frac{dc_{total}}{dt} \right)^* = \left( \sum Z_j^p - 1 \right) I\phi \frac{k_r}{k_d} c_{sub}. \quad (15)$$

Along with the photo-chemical reaction, the concentration gradient,  $\Delta c = c_{in} - c_{out}$ , across the membrane changes due to osmotic influx, and leak-out of the inner content through pore. Taking all the contribution into account and using principle of mass conservation for the solutes, we obtain

$$\frac{d(V\Delta c)}{dt} = V \left( \frac{dc_{total}}{dt} \right)^* - q_{out} A_p \Delta c - \frac{D}{R} A_p \Delta c. \quad (16)$$

Using Eqs. 9 and 15, the rate of change of the concentration difference is simplified as

$$\frac{d\Delta c}{dt} = \left( \sum Z_j^p - 1 \right) k c_{sub} - \frac{\Delta c}{V} \left( q_{in} A + \frac{D}{R} A_p \right), \quad (17)$$

where  $k = I\phi \frac{k_r}{k_d}$  is the effective rate constant for the substrate degradation, as described in Gandin et al. depends on experimental conditions<sup>38</sup>. Here,  $D$  is the solute diffusion coefficient. In Eq. 17, the first term on the right hand side represents molecular generation via the chemical reaction inside the vesicle, while the second term accounts for the concentration changes due to volume variation and diffusive contribution through pore leakage of the inner vesicle contents.

The three coupled equations, Eqs. 8, 10, and 17, constitute the continuum vesicle model with a stochastic approach to vesicle rupture and incorporating light-triggered reactions. To demonstrate the validity of our approach, we compare available experimental results, as reported in Chabanon et al., for time periods of swell-burst-reseal cycles against our model predictions<sup>15</sup>. In the absence of chemical reactions, we set  $k = 0$  and  $H_s = -0.001 \text{ nm}^{-1}$ . As shown in Fig. 2d, our model predictions are in good agreement with the experimental data. We note that in the dilute limit of solute molecules,  $H_s$  is small and does not alter the pulsatile behavior. However, as photo-chemical reactions generate a very high  $\Delta c$ , this assumption is no longer valid.

### 3 Model predictions and discussion

To determine  $\Delta c$  in the case of an active osmotic gradient, we need the effective rate constant  $k$  to account for the photo-chemical reactions. To this end, we use experimental images of Fig. 3a to extract  $R$  as plotted in Fig. 3b, corresponding to each of the vesicles. Before the pore opens (i.e.  $\alpha = 0$  from Fig. 2c), Eqs.

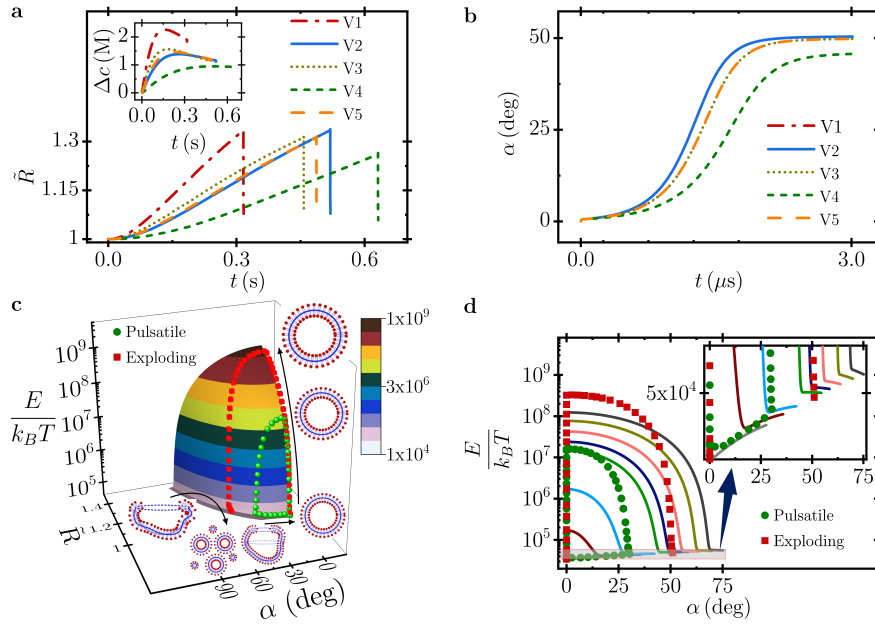


**Fig. 4 Model predictions of the pathway to vesicles explosion.** (a) Simulation results for  $\tilde{R} = R/R_0$ . The sudden drop of the area strain indicates lipid membrane rupture. Inset is  $\Delta c$  predicted by the model accounting for the chemical reaction. The osmotic gradient rises rapidly and remains constant until the membrane rupture. (b) Evolution of pore size under an active osmotic gradient. The simulations were performed for each of five vesicles. The model predicts a very large pore opening,  $\alpha \approx 50^\circ$ . Note that the time axis has been shifted to the initiation of the membrane rupture. (c) Dynamical paths followed by two vesicles rupturing at two different  $\varepsilon_a$  values: 80% (red cubes) and 20% (green spheres) plotted over the energy surface. Schematics of vesicle dynamics are shown at each stage. The black arrows are guides to the eyes. The vesicle rupturing at lower strain forms a loop indicative of pulsatile behavior (green spheres). However, the vesicle rupturing at higher strain jumps into the buckling regime, ultimately fragmenting into smaller daughter structures (red cubes). (d) Energy curves and dynamical paths in a 2D plane. Inset is a zoomed-in view of the shaded part to reveal the energy gradient at the maximum pore growth. A vesicle having a smaller pore faces adverse energy gradient (green circles), leading it to reseal. In the other case, a vesicle with a larger pore faces a favorable energy gradient (red squares), leading it to a buckling instability and ultimately exploding.

10-12 imply

$$\dot{R} = P V_s \left( \Delta c - \frac{\Delta p}{R_G T} \right), \quad (18)$$

which can be reverted to obtain total moles generated  $M_g$  as

$$M_g = \left( \frac{\dot{R}}{P V_s} + \frac{\Delta p}{R_G T} \right) \left( \frac{4}{3} \pi R^3 \right). \quad (19)$$

Using experimental data (Fig. 3b) and computing  $\Delta p$  from Eq. 6, we plot  $M_g$  against time (Fig. 3c). For  $\alpha = 0$  before the membrane ruptures, using Eqs. 9 and 17 we express the rate of change of the substrate concentration as

$$\frac{dc_{sub}}{dt} = -k c_{sub} - \frac{c_{sub}}{V} \frac{dV}{dt}. \quad (20)$$

Simplifying Eq. 20 with further algebraic manipulations, we obtain

$$\dot{M}_{sub} = -k M_{sub}. \quad (21)$$

From Eq. 21, the total substrate moles are  $M_{sub} = M_0 e^{-kt}$ , where  $M_0$  are the initial moles of the encapsulated substrate. Therefore, the total moles of substrate converted into the products follows  $M_0(1 - e^{-kt})$ . Furthermore, by multiplying the stoichiometric factor,  $\sum Z_j^p - 1$ , the total number of moles generated,  $M_g$ , inside a vesicle is written as

$$M_g = \left( \sum Z_j^p - 1 \right) M_0 \left( 1 - e^{-kt} \right), \quad (22)$$

We then fit the total moles generated to an exponential form  $A(1 - e^{-kt})$ , as predicted by Eq. 22, to extract the effective rate constant  $k$  (Fig. 3c).

After extracting the active osmotic gradient, we use our model to predict the vesicle dynamics, as shown in Figs. 4a, b. Figure 4a shows the evolution of the normalized vesicle radius  $\tilde{R} = R/R_0$ . We note that the evolution of  $\tilde{R}$  in Fig. 4a is smooth since there is only one instance of membrane rupture before disintegrating into several daughter structures. However, the stochasticity will be evident in a pulsatile regime with a series of swell-burst-reseal cycles. The sudden plunge in vesicle radius marks the instant of lipid membrane rupture. In simulations, we choose values of  $R/R_0$  at rupture similar to that obtained from experiments (Fig. 3b). The concentration difference  $\Delta c$  is shown in the inset of Fig. 4a. Note that the maximum  $\Delta c$  achieved here is  $\approx 2$  M, an order of magnitude higher than  $O(0.1)$  M in traditional passive osmotic gradient experiments<sup>15,18</sup>. For such a large osmotic gradient, the loading rate is in the range of 200 – 400 mN/m/s. This fact is corroborated by the rapid swelling in the experiments (Fig. 3a). Such a high  $\sigma$  is the key why a high strain,  $\varepsilon_a \approx 60 - 80\%$ , is allowed before rupture (Figs. 3b and 4a)<sup>20,22</sup>. Under these conditions, we expect the pore must grow very large. Indeed, as in Fig. 4b, simulations show a huge pore growth ( $\alpha \approx 50^\circ$ ). For a passive osmotic gradient,  $\varepsilon_a$  at rupture remains in the range of  $\approx 4 - 10\%$ <sup>11,12,18,31</sup>, and therefore relatively smaller pores are

formed given the smaller loading rates  $\approx 1$  mN/m/s.

To add further insights into why a large pore under an active osmotic gradient can lead to exploding, we examine the energy evolution of the vesicle system. We overlay the dynamical paths of two vesicles rupturing at two different strains, namely  $\varepsilon_a = 20\%$  (green spheres), and  $\varepsilon_a = 80\%$  (red cubes), on the energy surface of a vesicle system (Fig. 4c) considering all the configurations excluding the cases where the buckling instability occurs, *i.e.*  $\sigma < -24\pi k_b/A_0$ . Therefore, the bottom edge of the energy surface marks the buckling instability where the growth of the first mode of thermal undulations becomes unbounded<sup>39</sup>. As shown in Fig. 4c (green spheres), the vesicle rupturing at a small strain forms a closed loop, an implication of the characteristic swell-burst-reseal cycle. The vesicle rupturing at higher strain, however, shows an exploding behavior (red cubes).

Additionally, we show the energy curves with the dynamical paths in a 2D plane (Fig. 4d). As mentioned earlier, for the vesicle rupturing at smaller strain, the pore grows smaller than the case for the vesicle rupturing at larger strain. The inset of Fig. 4d displays the zoomed-in view of the shaded region of this plot. It shows that the vesicle rupturing at smaller strain (and thus smaller pore sizes) faces an adverse energy gradient at the end of the pore growth stage, helping vesicles to reseal (green circles, Fig. 4d). For the larger pore size, the energy gradient is favorable, transitioning the vesicle into the buckling regime (red squares, Fig. 4d). Consequently, as the undulations amplitude grows, the vesicle disintegrates into smaller daughter structures, showing an exploding behavior<sup>40–43</sup>.

We note that  $H_s = -0.011$  nm<sup>-1</sup> in our simulations for Fig. 4, which agrees well with the exploding experiments. Such a value is also consistent with the typical order of magnitude observed in the literature<sup>26</sup>. The spontaneous curvature develops as the lipid bilayer faces a large concentration difference across the membrane<sup>26</sup>. After the membrane ruptures, the vesicle is in a relaxed state, *i.e.*  $\sigma \approx 0$ , therefore leaving only the pore edge energy, to compete with the bending energy. Large negative  $H_s$  contributes to the excess bending energy, which dominates the pore edge energy at large pore sizes. Therefore, the vesicle prefers to unfold, driving it to the buckling instability and ultimately to its disintegration.

## 4 Conclusions

In this study, we have developed a semi-analytic approach to describe the mechanical response of semipermeable vesicles under the osmotic stress, integrating both pulsatile and exploding behaviors into a unified model. We have taken into account the stochastic nature of membrane rupture, as well as a variable osmotic gradient driven by chemical reactions. The considerations of the rate-dependent response of lipid bilayers and the spontaneous curvature are critical for explaining vesicle explosion. We have discussed different scenarios under hypo-osmotic shock conditions. In addition, our model could be potentially used in a hyper-osmotic environment as vesicles shrink to reach a buckling instability, in which the spontaneous curvature comes into play.

Photolytic chemical reactions provide an alternative to create hypotonic environments leading to membrane rupture regardless

of the physiological conditions of tissue. Tuning the chemical reaction, for example by choosing an appropriate chemical rate constant, can allow active manipulation of release mechanisms such as a slow and continuous release or an instant release of the encapsulated molecules on demand. Additionally, we could choose appropriate lipids to form vesicles to achieve a desired release rate, according to the pharmacokinetics of the therapeutics. Further experimental investigations are required to understand how membrane material properties and the chemical rate constant impact the optimal vesicle size range in which exploding might be possible.

In summary, our model advances the fundamental understanding of the bifurcation in vesicle dynamics. By being able to predict the conditions for different regimes, we have shown a new avenue toward the precise design of vesicle-based biomedical systems for many potential applications, such as localized delivery of cytotoxic drugs to target tumors with reduced systemic toxicity, or controlled deposition of functional nanoparticles in microfluidic devices for biomedical detection.

## Conflicts of interest

There are no conflicts to declare.

## Acknowledgements

V.K.M. and J.F. thank the partial support of Campus Research Board Award RB20014 of the University of Illinois at Urbana-Champaign. S.S. acknowledges partial support from the National Science Foundation under Grant No. CBET-1930691.

## References

- 1 S. Jeong, H. T. Nguyen, C. H. Kim, M. N. Ly and K. Shin, *Adv. Funct. Mater.*, 2020, **30**, 1907182.
- 2 K. Ogłęcka, P. Rangamani, B. Liedberg, R. S. Kraut and A. N. Parikh, *Elife*, 2014, **3**, e03695.
- 3 M. I. Angelova and I. Tsoneva, *Chem. Phys. Lipids*, 1999, **101**, 123–137.
- 4 E. K. Hoffmann, I. H. Lambert and S. F. Pedersen, *Physiol. Rev.*, 2009, **89**, 193–277.
- 5 H. Terasawa, K. Nishimura, H. Suzuki, T. Matsuura and T. Yomo, *Proc. Natl. Acad. Sci. U.S.A.*, 2012, **109**, 5942–5947.
- 6 K. Nishimura, T. Matsuura, T. Sunami, S. Fujii, K. Nishimura, H. Suzuki and T. Yomo, *RSC Adv.*, 2014, **4**, 35224–35232.
- 7 A. Samad, Y. Sultana and M. Aqil, *Curr. Drug Deliv.*, 2007, **4**, 297–305.
- 8 V. S. Malinin, P. Frederik and B. R. Lentz, *Biophys. J.*, 2002, **82**, 2090–2100.
- 9 A. P. Munuzuri, B. Busupalli and J. Perez-Mercader, *Langmuir*, 2018, **34**, 10984–10992.
- 10 C. Taupin, M. Dvolaitzky and C. Sauterey, *Biochemistry*, 1975, **14**, 4771–4775.
- 11 M. Koslov and V. Markin, *J. Theor. Biol.*, 1984, **109**, 17–39.
- 12 O. Sandre, L. Moreaux and F. Brochard-Wyart, *Proc. Natl. Acad. Sci. U.S.A.*, 1999, **96**, 10591–10596.
- 13 E. Karatekin, O. Sandre, H. Guitouni, N. Borghi, P.-H. Puech and F. Brochard-Wyart, *Biophys. J.*, 2003, **84**, 1734–1749.

- 14 M. A. Idiart and Y. Levin, *Phys. Rev. E*, 2004, **69**, 061922.
- 15 M. Chabanon, J. C. Ho, B. Liedberg, A. N. Parikh and P. Rangamani, *Biophys. J.*, 2017, **112**, 1682–1691.
- 16 T. F. Zhu and J. W. Szostak, *J. Syst. Chem.*, 2011, **2**, 4.
- 17 A. Peyret, E. Ibarboure, A. Tron, L. Beauté, R. Rust, O. Sandre, N. D. McClenaghan and S. Lecommandoux, *Angew. Chem. Int. Ed.*, 2017, **56**, 1566–1570.
- 18 S. Shin, V. S. Doan and J. Feng, *Phys. Rev. Appl.*, 2019, **12**, 024014.
- 19 Y. Elani, R. V. Law and O. Ces, *Nat. Commun.*, 2014, **5**, 5305.
- 20 E. Evans, V. Heinrich, F. Ludwig and W. Rawicz, *Biophys. J.*, 2003, **85**, 2342–2350.
- 21 S. A. Akimov, P. E. Volynsky, T. R. Galimzyanov, P. I. Kuzmin, K. V. Pavlov and O. V. Batishchev, *Sci. Rep.*, 2017, **7**, 12509.
- 22 E. Evans and B. A. Smith, *New J. Phys.*, 2011, **13**, 095010.
- 23 W. Helfrich, *Z. Naturforsch. C*, 1973, **28**, 693–703.
- 24 H. Deuling and W. Helfrich, *Biophys. J.*, 1976, **16**, 861–868.
- 25 W. Helfrich and R.-M. Servuss, *Il Nuovo Cimento D*, 1984, **3**, 137–151.
- 26 R. Lipowsky and H.-G. Döbereiner, *EPL*, 1998, **43**, 219.
- 27 S. T. Milner and S. Safran, *Phys. Rev. A*, 1987, **36**, 4371.
- 28 H. Deuling and W. Helfrich, *J. Phys. Paris*, 1976, **37**, 1335–1345.
- 29 R. Lipowsky, *Nature*, 1991, **349**, 475–481.
- 30 T. Taniguchi, *Phys. Rev. Lett*, 1996, **76**, 4444.
- 31 F. Brochard-Wyart, P. De Gennes and O. Sandre, *Physica A*, 2000, **278**, 32–51.
- 32 R. Ryham, I. Berezovik and F. S. Cohen, *Biophys. J.*, 2011, **101**, 2929–2938.
- 33 C. A. Aubin and R. J. Ryham, *J. Fluid Mech.*, 2016, **788**, 228–245.
- 34 R. J. Ryham, *J. Fluid Mech.*, 2018, **836**, 502–531.
- 35 W. Rawicz, K. Olbrich, T. McIntosh, D. Needham and E. Evans, *Biophys. J.*, 2000, **79**, 328–339.
- 36 R. Fettiplace and D. Haydon, *Physiol. Rev.*, 1980, **60**, 510–550.
- 37 I. E. Kochevar and R. W. Redmond, *Methods in Enzymology*, Elsevier, 2000, vol. 319, pp. 20–28.
- 38 E. Gandin, Y. Lion and A. Van de Vorst, *Photochem. Photobiol.*, 1983, **37**, 271–278.
- 39 W. K. den Otter, *J. Chem. Phys.*, 2005, **123**, 214906.
- 40 E. Boroske, M. Elwenspoek and W. Helfrich, *Biophys. J.*, 1981, **34**, 95–109.
- 41 H. Döbereiner, J. Käs, D. Noppl, I. Sprenger and E. Sackmann, *Biophys. J.*, 1993, **65**, 1396–1403.
- 42 A. J. Markvoort, A. Smeijers, K. Pieterse, R. van Santen and P. Hilbers, *J. Phys. Chem. B*, 2007, **111**, 5719–5725.
- 43 R. Wick, M. I. Angelova, P. Walde and P. L. Luisi, *Chem. Biol.*, 1996, **3**, 105–111.